Int J Physiol Pathophysiol Pharmacol 2018;10(2):115-123
www.ijppp.org /ISSN:1944-8171/IJPPP0075136

Original Article

Potential implication of SGK1-dependent activity change in BV-2 microglial cells

Hayato Asai, Koichi Inoue, Eisuke Sakuma, Yoshiaki Shinohara, Takatoshi Ueki

Department of Integrative Anatomy, Nagoya City University Graduate School of Medical Sciences, Nagoya 467-8601, Japan

Received February 28, 2018; Accepted April 9, 2018; Epub April 20, 2018; Published April 30, 2018

Abstract: It has recently been established that microglial activation is involved in the pathophysiology of various neurological and psychiatric disorders such as amyotrophic lateral sclerosis and schizophrenia. The pathological molecular machineries underlying microglial activation and its accelerating molecules have been precisely described in the diseased central nervous system (CNS). However, to date, the details of physiological mechanism, which represses microglial activation, are still to be elucidated. Our latest report demonstrated that serum- and glucocorticoid-inducible kinases (SGK1 and SGK3) were expressed in multiple microglial cell lines, and their inhibitor enhanced the toxic effect of lipopolysaccharide on microglial production of inflammatory substances such as TNFα and iNOS. In the present report, we prepared SGK1-lacked microglial cell line (BV-2) and demonstrated that deficiency of SGK1 in microglia induced its toxic conversion, in which it took amoeboid morphology characteristic of reactive microglia, increased CD68 expression, quickened its proliferation, and showed higher susceptibility to ATP and subsequent cell death. Our data indicate that SGK1 plays pivotal roles in inhibiting its pathological activation, and suggest its potential function as a therapeutic target for the treatment of various disorders related to the inflammation in the CNS.

Keywords: SGK1, microglia, inflammation, CRISPR/Cas9

Introduction

Recent studies have revealed that microglia play important roles in the function of the central nervous system under physiological and pathophysiological situations [1, 2]. They are derived from myelogenous cells distinct from other types of cells in the brain, and are supposed to be responsible for the immune system in the nervous system, in which blood-circulating immune cells are not eligible because of the blood-brain barrier. Microglial status is sustained relatively inactive under resting conditions, but they still work for maintenance of neuronal conditions and surveillance of infectious invaders [1]. They are then activated when extraordinary events take place, resulting in production and release of reactive oxygen species or inflammatory cytokines. These further facilitate inflammatory responses. Indeed, an administration of minocycline, which inhibits microglial activity, attenuates infarct volume induced by stroke and various symptoms of depression in animal models [3, 4]. In addition, the latest studies also show the impact of microglia in systemic regulation, such as blood pressure and body weight [5, 6], suggesting that microglial activation is associated not only with brain disorders but also with systemic disorganization.

Although inflammatory responses mediated by microglia in the brain are thus important, its molecular mechanism remains insufficiently understood. We recently found that SGK activity exacerbates the outcomes of ischemic brain injury in mice [7]. We then expanded the research of SGKs to non-neuronal cells in the neuronal system because the roles of SGKs in non-neuronal cells are uncertain [8]. In line with this, we reported that SGK1 and SGK3 are expressed in multiple microglial cell lines, and that SGK inhibition may enhance inflammatory responses induced by lipopolysaccharide (LPS) [8, 9]. Because the SGK inhibitor is likely to work on every SGK isoform [10-12], it is expect-

ed to distinguish the role of SGK subunits. We therefore attempt to abolish functional SGK1 using the clustered regularly interspaced palindromic repeats (CRISPR)/Cas9 system to investigate its serving significances precisely. To this end, we investigate how disruption of SGK1 may facilitate microglial activation.

Materials and methods

Reagents and antibodies

The following reagents and antibodies were used: lipopolysaccharide (LPS, Escherichia coli 111:B4, Sigma); protease inhibitor cocktail (Sigma); 3-(4,5-dimethylthiazol-2-yl)-2,5-diphenyltetrazoliumbromide (MTT, Wako); fluorescein diacetate (FDA, Wako); propidium iodide (PI, Wako); rat monoclonal antibody against CD68 (FA-11) conjugated with fluorescein isothiocyanate (FITC) (BioLegend); rabbit polyclonal antibody against actin (Sigma); rabbit polyclonal antibodies against SGK1, SGK3, phospho-Akt, and total Akt (Cell Signaling), GeneArt Precision gRNA Synthesis Kit (Thermo Fischer Scientific); Cas9 nuclease protein (Thermo Fisher Scientific).

Cell culture

A microglial cell line BV-2 was grown in Dulbecco's modified eagle medium with 5% fetal bovine serum and antibiotics.

Analyses of cellular morphology

Morphological analysis of BV-2 and the derivative was carried out by phase contrast images obtained with a microscope (Eclipse TS100, Nikon). Round cells were defined either as cells with no process or as cells, the longest process of which is shorter than the cell body diameter. The fields were randomly selected and 35-91 cells were examined in each field.

Plasmid construction

The cellular total RNA from adult C57BL/6 mouse brain was obtained using Isogen (Nippongene) according to the manufacturer's protocols [8, 13]. Single-strand cDNA synthesis was then performed using Revetrace (Funakoshi) according to the manufacturer's protocols. Polymerase chain reaction (PCR) was performed to obtain full-length mouse SGK1 with the above cDNA as a template. The PCR products were subcloned into pCMV-Tag2B (Stratagene). Those plasmids were transfected into cells using NEPA21 (NEPA Gene).

Quantitative real-time PCR

RNA extraction and cDNA synthesis were carried out as mentioned above. Quantitative real-time PCR was performed to validate the expression changes of selected genes using SYBR® Premix Ex Taq (TaKaRa) and the Thermal Cycler Dice Real Time System (Takara) in accordance with the manufacturer's protocols. The PCR amplification cycles consisted of denaturation at 95°C for 30 s, 40 cycles of denaturation at 95°C for 5 s, and annealing/extension at 60°C to for 30 s, followed by the detection of melt curve, 60°C-95°C. Real-time PCR reactions were carried out in duplicate for each sample and the average values were applied to the ΔΔCt method for data analysis. The primers used were described somewhere else [8].

Knockout of SGK1 in BV-2 cells

A target sequence (5'-CTTCTTGAAAGTGATCGGAA-3') was designed using Thermo Fisher CRISPR design tool (Thermo Fisher Scientific). A guide RNA was constructed using a GeneArt Precision gRNA Synthesis Kit (Thermo Fisher Scientific) according to the manufacturer's instruction. For the transfection, 5×10^4 cells were electroporated with 240 ng of the gRNA and 1 μg of Cas9 nuclease protein (Thermo Fisher Scientific) using an electroporator (1,700 V 10-msec pulse × 3, Neon™, Thermo Fisher Scientific). After single-cell isolation, monoclonal cell lines were obtained, genomic DNAs were extracted, and target regions were amplified by PCR using primer pairs for the expected mutation. The PCR products were inserted into pGEM T-easy vector (Promega) and sequenced.

Proliferation assay

Cells were plated into 24-well plates at 1×10^3 cells/well. Images of cells in randomly selected wells comprising 9 fields per well were snapped and those of the same fields were also obtained at 24-h intervals using IN Cell Analyzer 6000 (GE). In the case of transfected cells, 1×10^6 cells were transfected with 10 μg of the indicated plasmids and approximately 1/10 of those cells were placed in each well in 24-well plates. Images were deconvoluted using Developer software (GE) to recognize the cells

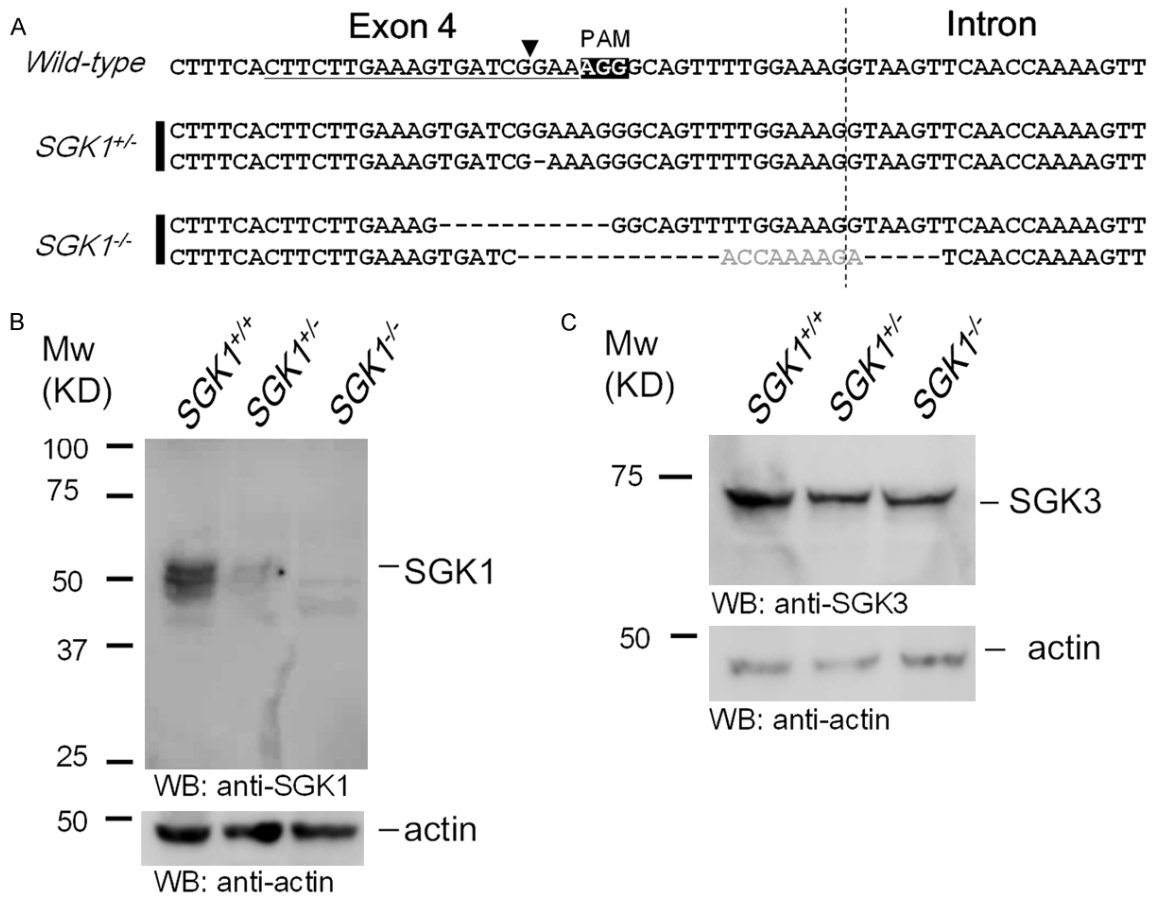

Figure 1. The *SGK1* gene is ablated by means of the CRISPR/Cas9 system. (A) The CRISPR/Cas9 system was applied to BV-2 cells, and mutations in *SGK1* exon 4 were obtained (see Materials and methods). The wild-type sequence is shown with a target site (underlined) of gRNA. A protospacer adjacent motif (PAM) is shown with white letters in a black box in the wild-type sequence. Expected cleavage site is indicated by arrowhead. Non-identical nucleotides are shown with gray letters. The border between exon 4 and the following intron is shown by a vertical dashed line. Dashes in the sequences represent deleted nucleotides. Those cells underwent immunoblotting using anti-SGK1 (B) and anti-SGK3 (C) antibodies. Protein loading was monitored with actin.

morphologically and the numbers of cells were counted.

MTT assay

MTT assay was done as described previously [8]. MTT solution was solved in phosphate-buffered saline (PBS) at a concentration of 5 mg/ml. Cells were seeded at 5 × 10^4 in 24-well plates. On the following day, cells were incubated with media (450 µl) in the presence or absence of ATP. Up to 24 h later, 50 µl of MTT solution was added into each well and incubated for 1 h. Media was then removed and 200 µl of 0.04 N HCl/2-propanol was added. They were transferred into 96-well plates and absorbance was measured at 570 nm with 690 nm as a reference using a microplate reader (Molecular Devices).

Cell death assay

FDA and PI staining was done as described previously [8]. Cells were seeded at 5 × 10^4 per well in 24-well plates. On the following day, cells were incubated with media in the absence or presence of 1 mM ATP. For staining of live and dead neurons, cultures were incubated with PBS containing FDA (3 µg/ml) and PI (5 µg/ml) for 5 min, followed by washing with PBS. Live (FDA-positive) and dead (PI-positive) cells were viewed with a fluorescence microscope (IX73, Olympus) at excitation/emission wavelengths of 470-495 nm/510-550 nm for FDA and 530-550 nm/575 nm for PI.

Immunocytochemistry

Cells were fixed with 4% paraformaldehyde in PBS, followed by incubation with 5% horse

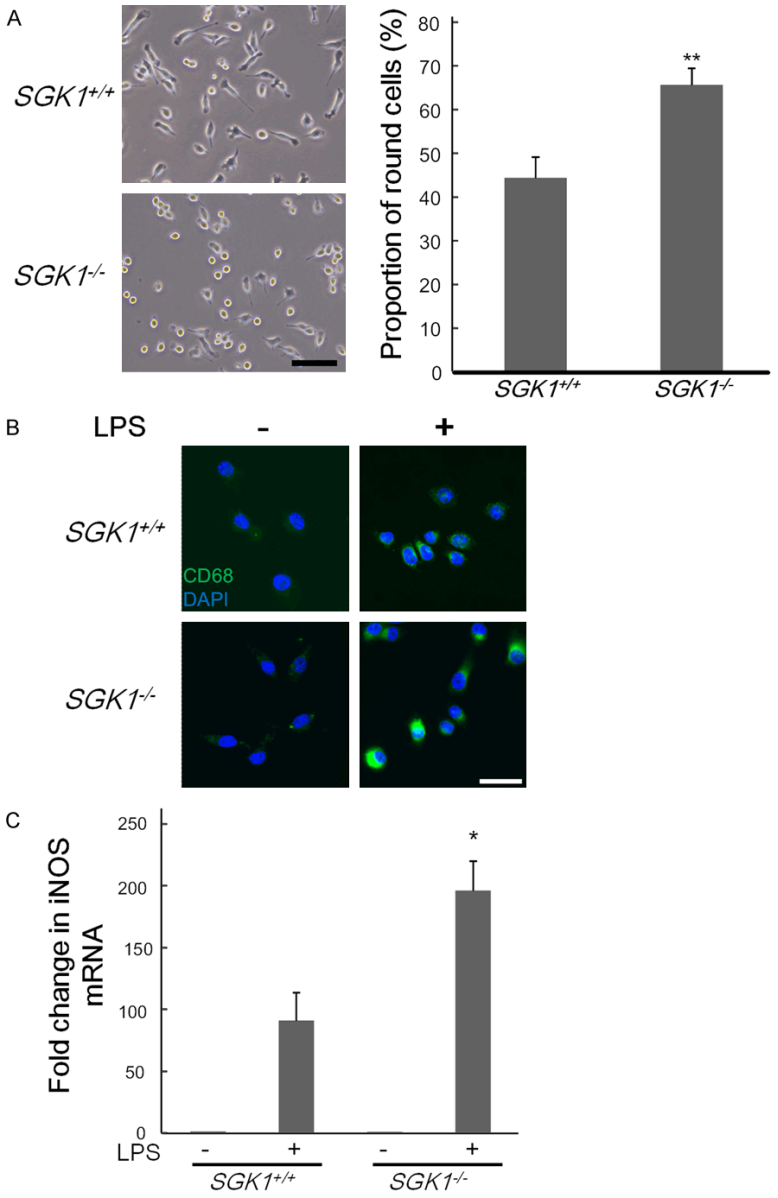

Figure 2. Disruption of the *SGK1* gene leads to activated features in BV-2 cells. A. Representative images of cells 24 h after being plated are shown. Scale bar; 100 μm. Bar chart indicates the proportion of round amoeboid-like cells. n = 9. **P < 0.01 vs *SGK1*$^{+/+}$ cells, Student's t-test. B. Cells were either untreated or treated with LPS (500 ng/ml) for 24 h, and then fixed. CD68 protein was visualized by immunofluorescence staining using an antibody for CD68 conjugated with FITC (green). For nuclear staining, the cells were stained with DAPI (blue). Representative images from three independent experiments were shown. Scale bar; 50 μm. C. Cells were incubated with LPS (500 ng/ml) for 4 h. After RNA extraction and reverse transcription to synthesize cDNA, quantitative real-time PCR was performed to monitor iNOS expression. n = 5-8. *P < 0.05 vs *SGK1*$^{+/+}$ cells, Student's t-test.

serum and 0.2% Triton X-100 in PBS at room temperature. The cells were then incubated with anti-CD68 antibody conjugated with FITC (1:1000). For DNA staining, coverslips were incubated with 4',6-diamidino-2-phenylindole (DAPI). Fluorescence images were collected using the above device and analyzed with HCImage software (Hamamatsu).

Immunoblotting

Immunoblotting was performed as described [14, 15]. Cells cultured on 35-mm dishes or 6-well plates were lysed in lysis buffer (50 mM Tris-HCl, pH 7.5, 150 mM NaCl, 1% Triton X-100, 12 μM β-glycerophosphate, 1 μM sodium orthovanadate, and protease inhibitor). After centrifugation at 15,000 × g at 4°C for 30 min, the lysates were collected. The aliquots were then mixed with Laemmli sample buffer and boiled at 95°C for 10 min. The samples were resolved by 10% SDS-PAGE, followed by electrotransfer to polyvinylidene difluoride membranes. For visualization, blots were probed with antibodies against SGK1 (1:1000), SGK3 (1:1000), phospho-Akt (Ser-473, 1:1000), total Akt (1:1000) or actin (1:2000), and detected using horseradish peroxidase-conjugated secondary antibodies (1:2000; Promega) and an ECL kit (Bio-RAD).

Statistical analysis

Data are presented as means ± SEM. Differences between groups were compared using one-way ANOVA, or unpaired Student's t-test as appropriate. Dunnett's test was used to compensate for multiple experimental procedures. P < 0.05 was regarded as statistically significant.

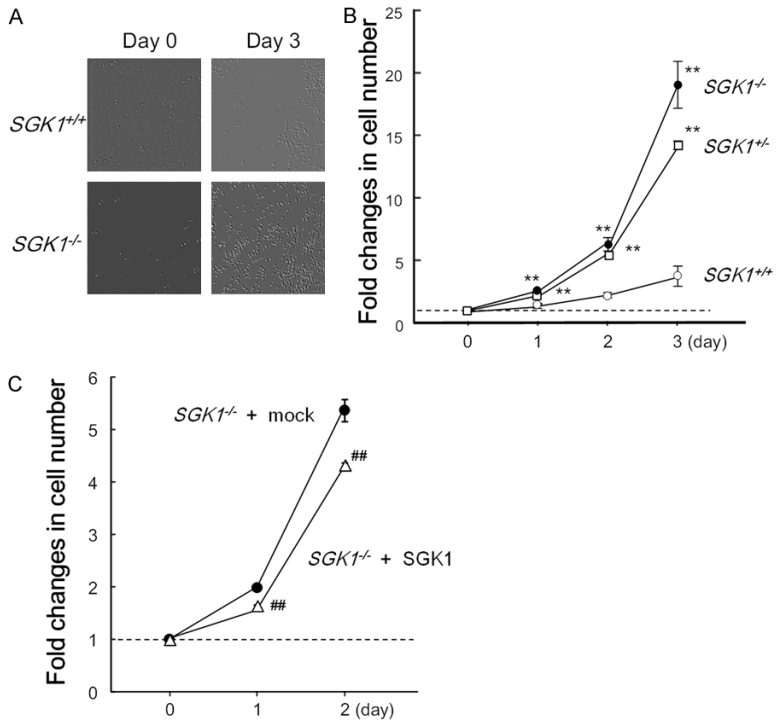

Figure 3. Breakdown of the *SGK1* gene facilitates proliferation rate. (A) Cells were seeded and the photos of the same fields were taken every 24 h. Representative images show cells in the same fields at day 0 and day 3. (B) The summary graph shows the fold changes in the normalized cell numbers of the indicated cells. n = 3-7 of independent dishes. $^{**}P < 0.01$ vs *SGK1*$^{+/+}$ cells in the same day, ANOVA followed by Dunnett's test. (C) *SGK1*$^{-/-}$ cells were transfected with SGK1-expressing vector (SGK1) or the control (mock), followed by cell counting described in (A). n = 4. $^{\#\#}P < 0.01$ vs mock, Student's t-test.

Results

Disruption of SGK1 in BV-2 cells

We have recently explored the presence and the significances of SGK1 and SGK3 in microglial cells [8]. To distinguish the role of SGK family members precisely, we aimed to create SGK1-disrupted cells from murine microglial cell line BV-2 cells, by employing the CRIPSR/Cas9 nuclease system [16, 17]. After targeting a region in exon 4, single clones were amplified and genomic DNAs were obtained. Sequential sequencing steps were carried out, and heterozygously and homozygously edited clones were obtained (**Figure 1A**). We then confirmed the deletion of SGK1 at the protein level. Immunoblotting analysis of cell extracts from these cells revealed that a ~50 kD band in agreement with SGK1 was detected in control BV-2 (*SGK1*$^{+/+}$) cells using anti-SGK1 antibody, while that of *SGK1*$^{-/-}$ cells did not display the corresponding band (**Figure 1B**). We also examined SGK3 at the protein level and it was not affected by knockout of the *SGK1* gene (**Figure 1C**).

Changes in morphology and CD68 expression in SGK1$^{-/-}$ *cells*

We first assessed the effect of SGK1 on morphology of microglial cells because inflammation affects its configuration [1, 18-20]. Up to 24 h after plating the cells, the majority of *SGK1*$^{+/+}$ cells showed a ramified shape with long process(es) (**Figure 2A**). However, most of the *SGK1*$^{-/-}$ cells exhibited a relatively round shape, which is characteristic of activated microglia (*SGK1*$^{+/+}$ cells; 44.4 ± 4.7%, n = 9, vs *SGK1*$^{-/-}$ cells 65.5 ± 3.9%, n = 9, P < 0.01, **Figure 2A**).

We also inspected the expression levels of CD68, an activation marker of microglial cells [21, 22]. Immunofluorescence analysis showed that *SGK1*$^{-/-}$ cells were positive for CD68 while *SGK1*$^{+/+}$ cells were relatively less labelled (**Figure 2B**). When cells were treated with LPS, CD68 signals were elevated in both cells and *SGK1*$^{-/-}$ cells provided more intensive signals than *SGK1*$^{+/+}$ cells did. These results suggest that disruption of SGK1 encourages microglial activation (**Figure 2B**).

The effect of SGK1 disruption on iNOS gene expression induced by LPS

To test whether loss of SGK1 affects inflammatory response, LPS-induced iNOS gene expression was determined. Basal levels of iNOS mRNA were not different between *SGK1*$^{+/+}$ and *SGK1*$^{-/-}$ (*SGK1*$^{+/+}$ cells; 1.0 ± 0.9 fold, n = 8, vs *SGK1*$^{-/-}$ cells; 0.9 ± 0.5 fold, n = 5, P > 0.05, **Figure 2C**). Interestingly, LPS augmented iNOS expression to a greater extent in *SGK1*$^{-/-}$ cells than in *SGK1*$^{+/+}$ cells (*SGK1*$^{+/+}$ cells; 90.9 ± 22.6 fold, n = 8, vs *SGK1*$^{-/-}$ cells; 196.0 ± 23.7 fold, n

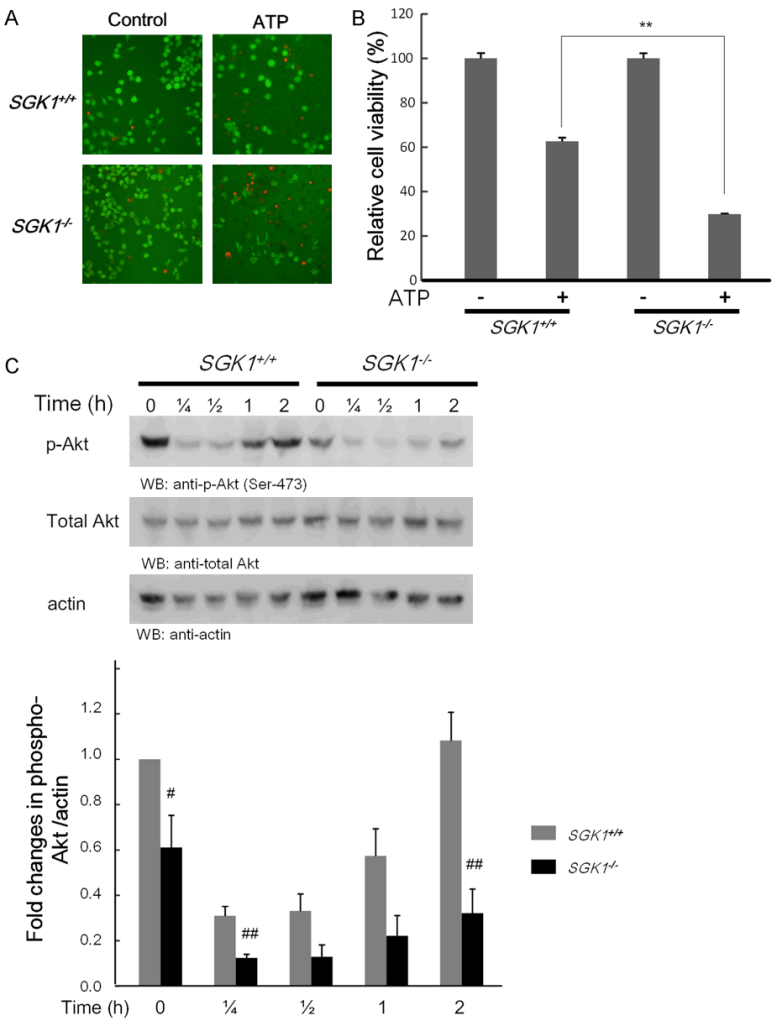

Figure 4. Loss of the *SGK1* gene results in vulnerability to ATP-induced damage. Cells were untreated or treated with 1 mM ATP for 24 h. A. Photo images show cells stained with fluorescein (green; for live cells) and PI (red; for injured cells). *SGK1*$^{-/-}$ cells are likely to show a greater amount of PI-positive cells. B. MTT values were assessed. The values of the *SGK1*$^{-/-}$ cells treated with ATP were lower than those of the *SGK1*$^{+/+}$ cells. Taken together, these results suggest *SGK1*$^{-/-}$ cells are more susceptible to ATP-induced cellular damage. n = 4, $^{**}P < 0.01$ vs *SGK1*$^{+/+}$ cells, Student's t-test. C. Cells were treated with 1 mM ATP for the indicated periods. Cell lysates then underwent immunoblotting analysis with phospho-Akt (Ser-473) and total Akt antibodies. Bar graph shows the signal intensities quantified by densitometric analysis. Phospho-Akt signals were normalized for actin, and the value of *SGK1*$^{+/+}$ cells at *t* = 0 was set as the basal level. n = 4-5. $^{\#}P < 0.05$, $^{\#\#}P < 0.01$ vs *SGK1*$^{+/+}$ cells, Student's t-test.

= 5, compared with untreated *SGK1*$^{+/+}$ cells, P < 0.05, **Figure 2C**). This pattern is consistent with our previous study that an SGK inhibitor promoted LPS-induced iNOS expression [8].

The effect of SGK1 disruption on proliferation

We then evaluated whether growth is influenced by ablation of the *SGK1* gene. After the cells were seeded on plates, the fields were randomly selected and the corresponding fields were sequentially examined every 24 h. As shown in **Figure 3A** and **3B**, *SGK1*$^{-/-}$ cells grew faster than *SGK1*$^{+/+}$ cells, and the growth rate of the *SGK1*$^{+/-}$ cells was intermediate.

Although this suggests that SGK1 slows proliferation under normal conditions, an off-target effect could still be considerable at this point. To rule out the possibility of the off-target effect, a plasmid expressing SGK1 was transfected into *SGK1*$^{-/-}$ cells and the differences of proliferation were assessed. As shown in **Figure 3C**, the cells with SGK1 displayed slower proliferation compared with the cells transfected with mock vector. Thus, this further supports the idea that loss of SGK1 facilitates proliferation.

Susceptibility to ATP-mediated cellular injury by disruption of the SGK1 gene

Activation of microglial cells accompanies susceptibility to various stimuli [1]. To examine whether elimination of SGK1 affects susceptibility of cells to stress, we decided to apply ATP. ATP is anticipated to be released by surrounding cells, and high doses of ATP cause cellular damage, such as traumatic or ischemic injuries [19]. This activates microglial cells, facilitating proliferation subsequently apoptosis [1, 19]. Application of ATP to BV-2 cells resulted in damage, as expected (**Figure 4A**). Of note, although *SGK1*$^{-/-}$ cells were also found to be injured, a larger number of them was likely to be damaged (**Figure 4A**). We then investigated quantitative vulnerability using MTT assay. As a result, MTT

values of *SGK1*$^{-/-}$ cells treated with ATP dropped dramatically (29.7 ± 4.1%, n = 4), while those of *SGK1*$^{+/+}$ cells did so only moderately (62.6 ± 1.6%, n = 4). These results thus suggest that *SGK*$^{-/-}$ cells were more susceptible to ATP than *SGK1*$^{+/+}$ cells (**Figure 4B**).

To determine the mechanism by which loss of SGK1 augments vulnerability to ATP, we examined phosphorylation levels of Akt, because high doses of ATP are known to repress Akt signaling in microglial and other cells [23, 24]. The basal level of phosphorylation of Akt was significantly lower in *SGK1*$^{-/-}$ cells compared with *SGK1*$^{+/+}$ cells (**Figure 4C**). Moreover, the phosphorylation level of Akt was restored at 2 h after ATP administration in *SGK1*$^{+/+}$ cells, whereas the recovery in *SGK1*$^{-/-}$ cells was delayed (**Figure 4C**). Taken together, increased susceptibility of *SGK1*$^{-/-}$ cells against ATP-induced cellular injury may be at least partly due to lesser activity of Akt signaling.

Discussion

Considering the consequence of SGK1 in different mammalian organs, the focus of its roles in earlier studies has mainly been on renal function regarding Na^+ reabsorption in which epithelial Na^+ channels are regulated by an E3 ubiquitin ligase Nedd4-2 [25-27]. While its function has been uncovered less in neurobiology, cumulative evidence shows the enrollment of SGK1 in neuroscience, in which, for example, neuronal SGK1 plays roles in fear retention and working memory [28, 29]. In addition, recent studies have further explored the roles of SGK1 in glial cells, such as astrocytes and oligodendrocytes [30-32]. However, few studies have examined SGKs in microglial cells, with one finding that SGK1 is present in a small number of microglial cells [33].

We have recently reported the expression and the roles of SGK1 and SGK3 in microglial inflammatory responses [8]. However, for an SGK inhibitor, which is expected to block activity of both SGK isoforms [10, 12], the subunit-dependent roles were not segregated. We showed SGK1-specific roles in microglial cells by disruption of the *SGK1* gene in this study. We have observed enhancement of LPS-induced CD68 and iNOS expression, amoeboid-like morphology, growth rate, and susceptibility to ATP stimulation in *SGK1*$^{-/-}$ cells, and these incidences corresponded to the ones seen in microglial cells activated by stimuli [1, 19, 34]. This suggests that SGK1 may take part in the inhibition of activation and inflammation at the basal level. Interestingly, as shown in **Figure 4C**, we found that depletion of SGK1 diminishes phosphorylation of Akt, which means that SGK1 facilitates Akt signaling. This can explain the mechanism by which *SGK1*$^{-/-}$ exhibits higher sensitivity to ATP-induced damage. Although the precise mechanism still needs to be determined, excess of microglial activation could be controlled, if stimuli that upregulate SGK1 expression without side effects are administrated. SGK1 is known to be induced by glucocorticoids in a variety of cells from which the name derives [25], but, unexpectedly, dexamethasone did not induce it in BV-2 cells (data not shown). The inducing factors of SGK1 in microglial cells might be different from that in other cells as an earlier study showed that an increase in corticosterone does not appear to raise microglial SGK1 [35]. As well as the molecular mechanism of SGK1-dependent microglial activity, seeking molecules regulating SGK1 expression and whether phenomena shown in this study can be observed in vivo should be investigated in future.

Acknowledgements

We thank Mr. H. Takase for technical assistance. This work was supported by a KAKENHI Grant-in-Aid for Scientific Research No. 16K-09520, Salt Science Research Foundation Grant 1721 (K.I.), and KAKENHI Grant-in-Aid for Scientific Research on Innovative Areas "Willdynamics" (16H06404) (K.I. and T.U.).

Disclosure of conflict of interest

None.

Address correspondence to: Koichi Inoue and Takatoshi Ueki, Department of Integrative Anatomy, Nagoya City University Graduate School of Medical Sciences, Nagoya 467-8601, Japan. Tel: +81-52-853-8121; Fax: +81-52-853-8122; E-mail: ino-k@umin.ac.jp (KI); ueki@med.nagoya-cu.ac.jp (TU)

References

[1] Kettenmann H, Hanisch UK, Noda M and Verkhratsky A. Physiology of microglia. Physiol Rev 2011; 91: 461-553.

[2] Aloisi F. Immune function of microglia. Glia 2001; 36: 165-179.
[3] Yenari MA, Kauppinen TM and Swanson RA. Microglial activation in stroke: therapeutic targets. Neurotherapeutics 2010; 7: 378-391.
[4] Yrjänheikki J, Tikka T, Keinänen R, Goldsteins G, Chan PH and Koistinaho J. A tetracycline derivative, minocycline, reduces inflammation and protects against focal cerebral ischemia with a wide therapeutic window. Proc Natl Acad Sci U S A 1999; 96: 13496-13500.
[5] Shen XZ, Li Y, Li L, Shah KH, Bernstein KE, Lyden P and Shi P. Microglia participate in neurogenic regulation of hypertension. Hypertension 2015; 66: 309-316.
[6] Andre C, Guzman-Quevedo O, Rey C, Remus-Borel J, Clark S, Castellanos-Jankiewicz A, Ladeveze E, Leste-Lasserre T, Nadjar A, Abrous DN, Laye S and Cota D. Inhibiting microglia expansion prevents diet-induced hypothalamic and peripheral inflammation. Diabetes 2017; 66: 908-919.
[7] Inoue K, Leng T, Yang T, Zeng Z, Ueki T and Xiong ZG. Role of serum- and glucocorticoid-inducible kinases in stroke. J Neurochem 2016; 138: 354-361.
[8] Inoue K, Sakuma E, Morimoto H, Asai H, Koide Y, Leng T, Wada I, Xiong ZG and Ueki T. Serum- and glucocorticoid-inducible kinases in microglia. Biochem Biophys Res Commun 2016; 478: 53-59.
[9] Inoue K. Possible divergence of serum- and glucocorticoid-inducible kinase function in ischemic brain injury. Neural Regen Res 2016; 11: 1396-1397.
[10] Sherk AB, Frigo DE, Schnackenberg CG, Bray JD, Laping NJ, Trizna W, Hammond M, Patterson JR, Thompson SK, Kazmin D, Norris JD and McDonnell DP. Development of a small-molecule serum- and glucocorticoid-regulated kinase-1 antagonist and its evaluation as a prostate cancer therapeutic. Cancer Res 2008; 68: 7475-7483.
[11] Ackermann TF, Boini KM, Beier N, Scholz W, Fuchss T and Lang F. EMD638683, a novel SGK inhibitor with antihypertensive potency. Cell Physiol Biochem 2011; 28: 137-146.
[12] Wang Y, Zhou D, Phung S, Warden C, Rashid R, Chan N and Chen S. SGK3 sustains ERa signaling and drives acquired aromatase inhibitor resistance through maintaining endoplasmic reticulum homeostasis. Proc Natl Acad Sci U S A 2017; 114: E1500-E1508.
[13] Inoue K, Ueno S, Yamada J and Fukuda A. Characterization of newly cloned variant of rat glycine receptor alpha1 subunit. Biochem Biophys Res Commun 2005; 327: 300-305.
[14] Inoue K, Branigan D and Xiong ZG. Zinc-induced neurotoxicity mediated by transient receptor potential melastatin 7 channels. J Biol Chem 2010; 285: 7430-7439.
[15] Inoue K, Furukawa T, Kumada T, Yamada J, Wang T, Inoue R and Fukuda A. Taurine inhibits K^+-Cl^- cotransporter KCC2 to regulate embryonic Cl^- homeostasis via with-no-lysine (WNK) protein kinase signaling pathway. J Biol Chem 2012; 287: 20839-20850.
[16] Ran FA, Hsu PD, Wright J, Agarwala V, Scott DA and Zhang F. Genome engineering using the CRISPR-Cas9 system. Nat Protoc 2013; 2281-2308.
[17] Sander JD and Joung JK. CRISPR-Cas systems for editing, regulating and targeting genomes. Nat Biotechnol 2014; 32: 347-355.
[18] Cizkova D, Devaux S, Le Marrec-Croq F, Franck J, Slovinska L, Blasko J, Rosocha J, Spakova T, Lefebvre C, Fournier I and Salzet M. Modulation properties of factors released by bone marrow stromal cells on activated microglia: an in vitro study. Sci Rep 2014; 4: 7514.
[19] Lee S, Lee J, Kim S, Park JY, Lee WH, Mori K, Kim SH, Kim IK and Suk K. A dual role of lipocalin 2 in the apoptosis and deramification of activated microglia. J Immunol 2007; 179: 3231-3241.
[20] McHugh D, Roskowski D, Xie S and Bradshaw HB. D^9-THC and *N*-arachidonoyl glycine regulate BV-2 microglial morphology and cytokine release plasticity: implications for signaling at GPR18. Front Pharmacol 2014; 4: 162.
[21] Kwon YW, Cheon SY, Park SY, Song J and Lee JH. Tryptanthrin suppresses the activation of the LPS-Treated BV2 microglial cell line via Nrf2/HO-1 antioxidant signaling. Front Cell Neurosci 2017; 11: 18.
[22] Girard S, Brough D, Lopez-Castejon G, Giles J, Rothwell NJ and Allan SM. Microglia and macrophages differentially modulate cell death after brain injury caused by oxygen-glucose deprivation in organotypic brain slices. Glia 2013; 61: 813-824.
[23] Bian S, Sun X, Bai A, Zhang C, Li L, Enjyoji K, Junger WG, Robson SC and Wu Y. P2X7 integrates PI3K/AKT and AMPK-PRAS40-mTOR signaling pathways to mediate tumor cell death. PLoS One 2013; 8: e60184.
[24] Hao F, Zhang NN, Zhang DM, Bai HY, Piao H, Yuan B, Zhu HY, Yu H, Xiao CS and Li AP. Chemokine fractalkine attenuates overactivation and apoptosis of BV-2 microglial cells induced by extracellular ATP. Neurochem Res 2013; 38: 1002-1012.
[25] Webster MK, Goya L, Ge Y, Maiyar AC and Firestone GL. Characterization of sgk, a novel member of the serine/threonine protein kinase gene family which is transcriptionally induced by glucocorticoids and serum. Mol Cell Biol 1993; 13: 2031-2040.

[26] Debonneville C, Flores SY, Kamynina E, Plant PJ, Tauxe C, Thomas MA, Munster C, Chraibi A, Pratt JH, Horisberger JD, Pearce D, Loffing J and Staub O. Phosphorylation of Nedd4-2 by Sgk1 regulates epithelial Na^+ channel cell surface expression. EMBO J 2001; 20: 7052-7059.

[27] Lang F, Bohmer C, Palmada M, Seebohm G, Strutz-Seebohm N and Vallon V. (Patho)physiological significance of the serum- and glucocorticoid-inducible kinase isoforms. Physiol Rev 2006; 86: 1151-1178.

[28] Lee CT, Ma YL and Lee EH. Serum- and glucocorticoid-inducible kinase1 enhances contextual fear memory formation through down-regulation of the expression of Hes5. J Neurochem 2007; 100: 1531-1542.

[29] Yuen EY, Liu W, Karatsoreos IN, Ren Y, Feng J, McEwen BS and Yan Z. Mechanisms for acute stress-induced enhancement of glutamatergic transmission and working memory. Mol Psychiatry 2011; 16: 156-170.

[30] Miyata S, Hattori T, Shimizu S, Ito A and Tohyama M. Disturbance of oligodendrocyte function plays a key role in the pathogenesis of schizophrenia and major depressive disorder. Biomed Res Int 2015; 2015: 492367.

[31] Miyata S, Koyama Y, Takemoto K, Yoshikawa K, Ishikawa T, Taniguchi M, Inoue K, Aoki M, Hori O, Katayama T and Tohyama M. Plasma corticosterone activates SGK1 and induces morphological changes in oligodendrocytes in corpus callosum. PLoS One 2011; 6: e19859.

[32] Koyanagi S, Kusunose N, Taniguchi M, Akamine T, Kanado Y, Ozono Y, Masuda T, Kohro Y, Matsunaga N, Tsuda M, Salter MW, Inoue K and Ohdo S. Glucocorticoid regulation of ATP release from spinal astrocytes underlies diurnal exacerbation of neuropathic mechanical allodynia. Nat Commun 2016; 7: 13102.

[33] Wärntges S, Friedrich B, Henke G, Duranton C, Lang PA, Waldegger S, Meyermann R, Kuhl D, Speckmann EJ, Obermuller N, Witzgall R, Mack AF, Wagner HJ, Wagner A, Broer S and Lang F. Cerebral localization and regulation of the cell volume-sensitive serum- and glucocorticoid-dependent kinase SGK1. Pflugers Arch 2002; 443: 617-624.

[34] Liu JL, Tian DS, Li ZW, Qu WS, Zhan Y, Xie MJ, Yu ZY, Wang W and Wu G. Tamoxifen alleviates irradiation-induced brain injury by attenuating microglial inflammatory response in vitro and in vivo. Brain Res 2010; 1316: 101-111.

[35] Hinds LR, Chun LE, Woodruff ER, Christensen JA, Hartsock MJ and Spencer RL. Dynamic glucocorticoid-dependent regulation of *Sgk1* expression in oligodendrocytes of adult male rat brain by acute stress and time of day. PLoS One 2017; 12: e0175075.